The Astrophysical Journal Letters, 811:L17 (6pp), 2015 October 1 doi:10.1088/2041-8205/811/2/L17

SPECTRAL ANALYSIS OF MAGNETIC FLUCTUATIONS AT PROTON SCALES FROM FAST TO SLOW SOLAR WIND

R. Bruno[1] and D. Telloni[2]
[1] National Institute for Astrophysics, Institute for Space Astrophysics and Planetology, Via del Fosso del Cavaliere 100, I-00133 Roma, Italy
[2] National Institute for Astrophysics, Astrophysical Observatory of Torino, Via Osservatorio 20, I-10025 Pino Torinese, Italy
Received 2015 June 8; accepted 2015 August 1; published 2015 September 23

ABSTRACT

This Letter investigates the spectral characteristics of interplanetary magnetic field fluctuations at proton scales during several time intervals chosen along the speed profile of a fast stream. The character of the fluctuations within the first frequency decade, beyond the high-frequency break located between the fluid and kinetic regimes, strongly depends on the type of wind. While the fast wind shows a clear signature of both right-handed and left-handed polarized fluctuations, possibly associated with Kinetic Alfvén Wave (KAW) and ion-cyclotron waves, respectively, the rarefaction region, where the wind speed and the Alfvénicity of low-frequency fluctuations decrease, shows a rapid disappearance of the ion-cyclotron signature followed by a more gradual disappearance of KAWs. Moreover, the power associated with perpendicular and parallel fluctuations also experiences rapid depletion, however, retaining the power anisotropy in favor of the perpendicular spectrum.

Key words: interplanetary medium – magnetic fields – plasmas – solar wind – turbulence – waves

1. INTRODUCTION

Interplanetary magnetic field fluctuations show a clear turbulent spectrum characterized by a well-established Kolmogorov scaling (see the reviews by Tu & Marsch 1995; Bruno & Carbone 2013 and references therein). Energy cascades from the largest energy-containing eddies to the high-frequency region of the spectrum where wave-particle interactions energize the ions at scales comparable to the typical proton scales (Marsch 2012).

The temperature anisotropy shown by the proton velocity distribution, as well as the preferential heating and acceleration of minor ions (see the review by Marsch 2006), are clear indicators of the coupling between the magnetic energy of the fluctuations and the kinetic energy of the ions. The result of this energy transfer is a steepening of the spectral index, which marks the beginning of the kinetic range (Denskat et al. 1983); however, a steepening of the spectrum at proton scales can also be obtained without invoking dissipation while taking into account the Hall effect (Galtier & Buchlin 2007). The location of this high-frequency break depends on the local magnetic field and plasma conditions, and varies with the heliocentric distance moving to lower frequencies as the wind expands, as shown by Bruno & Trenchi (2014). These authors concluded that an ion-cyclotron resonance dissipation mechanism, in which the Doppler-shifted frequency matches the particle gyrofrequency, must participate in the spectral cascade together with other possible kinetic non-resonant mechanisms, such as Landau damping acting on the perpendicular short-scale fluctuations generated by the large-scale eddies.

On the other hand, the nature of the fluctuations within the kinetic range is still debated (Alexandrova et al. 2013). The fact that one of the properties of the transition range separating the fluid from the kinetic regime is represented by an increase in compressibility (Alexandrova et al. 2008) suggests the presence of Kinetic Alfvén Waves (KAWs, hereafter; Leamon et al. 1998; Alexandrova et al. 2008; Hamilton et al. 2008; Sahraoui et al. 2009; Turner et al. 2011; Kiyani et al. 2013) and/or whistler waves (Gary & Borovsky 2004; Gary & Smith 2009; TenBarge et al. 2012). In this respect, Salem et al. (2012), using Cluster observations in the solar wind, showed that the properties of the small-scale fluctuations are inconsistent with the whistler wave model, but strongly agree with the prediction of a spectrum of KAWs with nearly perpendicular wavevectors.

Moreover, Alexandrova et al. (2008) reported that the intermittent character of magnetic field fluctuations within the kinetic range increases toward smaller scales and persists at least to electron scales (Perri et al. 2012; Wan et al. 2012; Karimabadi et al. 2013), indicating the presence of coherent magnetic structures advected by the solar wind. Further analyses associated elevated plasma temperature and anisotropy events with these structures, suggesting that inhomogeneous dissipation was at work (Servidio et al. 2012). Partially at odds with these results, Wu et al. (2013), using both flux-gate and search-coil magnetometers on board *Cluster*, found kinetic scales that are much less intermittent than fluid scales. These authors recorded a remarkable and sudden decrease back to near-Gaussian values of intermittency around scales of about 10 times the ion inertial scale, followed by a modest increase moving toward electron scales, in agreement with Kiyani et al. (2009), who showed observational results suggesting a scale-invariance within the small-scale range.

Other authors (He et al. 2011, 2012a, 2012b; Podesta & Gary 2011) studied the polarization state of the fluctuations within the kinetic regime, adopting a wavelet transform of the reduced magnetic helicity (Matthaeus & Goldstein 1982; Bruno et al. 2008) observed in a plane perpendicular to the sampling direction. This kind of analysis was performed for different pitch angles θ_{VB} between the the flow direction and the local mean magnetic field (Horbury et al. 2008).

These authors found left-handed Alfvén/ion-cyclotron waves propagating outward almost parallel to the local magnetic field and right-handed KAWs propagating at large angles which confirmed previous conclusions by Goldstein et al. (1994), Leamon et al. (1998), and Hamilton et al. (2008) about the presence of KAWs.

In a recent study, Telloni et al. (2015) found that the spectral locations of these two populations follow the frequency shift

experienced by the high-frequency spectral break during the radial expansion of the wind (Bruno & Trenchi 2014). This behavior was interpreted as further experimental evidence relating the presence of these fluctuations to the location of the frequency break. The same authors suggested that the decrease in intermittency beyond the spectral break might be caused by the stochastic nature of these fluctuations. Finally, Bruno et al. (2014) showed that the spectral slope is generally higher whenever the power level (and/or the Alfvénic character) of the fluctuations is higher within the inertial range. They suggested that the behavior of the spectral slope might be related to some dissipative mechanism, such as Landau damping and/or ion-cyclotron resonance.

Consequently, it is interesting to verify whether the polarization of the fluctuations changes when we move from fast to slow wind within the same high-speed stream given that fluctuations in the inertial range are progressively characterized by different Alfvénicity, compressibility, and intermittency (Bruno & Carbone 2013). This is the main goal of the present study.

2. DATA ANALYSIS AND RESULTS

We adopt the same data analysis techniques reported in Telloni et al. (2015) to study the polarization character of the fluctuations at kinetic scales as a function of the pitch angle between the sampling direction and the local magnetic field direction. The study will be performed scale by scale, sampling different field and plasma intervals along the wind speed profile, from fast to slow wind. We chose a fast wind stream observed by *WIND* between the end of 2010 June and the beginning of 2010 July; the same stream was studied in Telloni et al. (2015). High-resolution magnetic field measurements at about 92 ms were taken by the Magnetic Field Instrument (Lepping et al. 1995) on board *Wind*, while 1minute plasma measurements were performed by the Solar Wind Experiment (Ogilvie et al. 1995). Both data sets are available at the NASA-CDAWEB facility.

The speed profile of this fast wind stream is characterized by large amplitude velocity fluctuations within the trailing edge and much smaller fluctuations within the following rarefaction region (Hundhausen 1972) where the speed decreases faster. These strong fluctuations are intimately related to the presence of large amplitude Alfvénic fluctuations (Matteini et al. 2014), as can be inferred from Figure 1 where we show the speed profile together with the value of the correlation coefficient C_{VB} (Bavassano et al. 1998). This parameter estimates the correlation level between the magnetic field and velocity fluctuations expressed as $C_{VB} = \sigma_c / \sqrt{1 - \sigma_r^2}$, where σ_c and σ_r are the normalized forms of cross-helicity and residual energy, respectively (Bruno & Carbone 2013), and $\sigma_r \neq \pm 1$. The parameter C_{VB} has been evaluated on a timescale of 1 hr and, for graphical reasons, results have successively been smoothed with a 12 hr sliding average. Thus, C_{VB} shows the level of Alfvénic correlations along the speed profile of this stream. Before the beginning of DoY 184, C_{VB} is largely above 0.5 in magnitude. Afterward, this parameter experiences a fast decrease toward 0, especially within the stream rarefaction region. The positive sign of the correlation indicates that the Alfvénic fluctuations have an outward sense of propagation since the background magnetic field is inwardly directed.

We recall briefly the definitions and the technique we used; we suggest that readers refer to Telloni et al. (2015) for a more

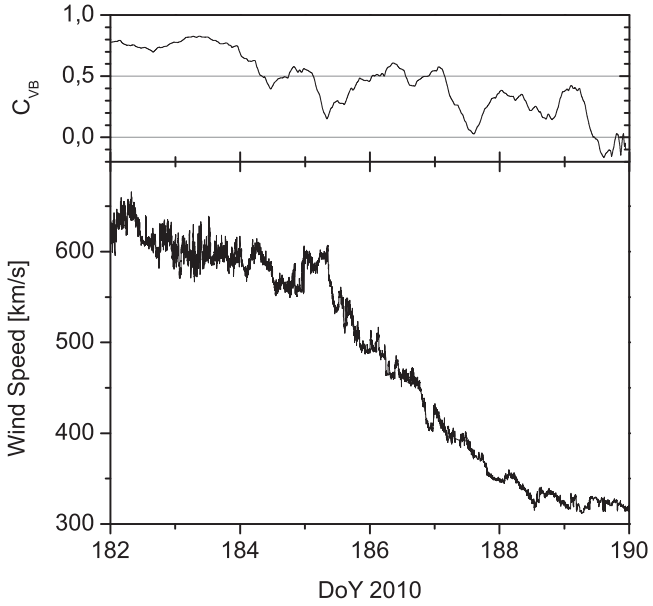

Figure 1. Top panel: time profile of the correlation factor C_{VB} on a scale of 1 hr and smoothed out with a 12 hr sliding window. Bottom panel: wind speed profile at a time resolution of 1 minute.

detailed discussion. The polarization of the fluctuations can be studied using the normalized reduced magnetic helicity σ_m (Matthaeus & Goldstein 1982). This measurable can be investigated based on both time t and temporal scale τ using wavelet transforms (Torrence & Compo 1998), as suggested by Bruno et al. (2008) and successively adopted by He et al. (2011, 2012a, 2012b) and Podesta & Gary (2011).

The normalized reduced magnetic helicity $\sigma_m(t, \tau)$ varies between $+1$ and -1, with positive and negative signs for the left and right circular polarizations, respectively. For an inward-oriented background magnetic field, assuming outward propagation, a left-handed ion-cyclotron waves would have a positive magnetic helicity. The same wave would result in negative helicity for an outward-oriented magnetic field (Narita et al. 2009; He et al. 2011). Thus, it is necessary to know the angle θ_{VB} between the sampling direction assumed along the wind direction and the magnetic field, scale by scale. In order to do so, we first reorder all of the values of $\sigma_m(t, \tau)$ into values of $\sigma_m(\theta_{VB}, \tau)$. Then, to determine the local magnetic field scale by scale, we operate a convolution between a Gaussian (normalized to unity), whose width is equal to the scale τ, and the magnetic field $\boldsymbol{B}_0(t)$ (Horbury et al. 2008; He et al. 2011; Podesta & Gary 2011). Finally, all of the values of $\sigma_m(t, \tau)$ found within the same angular bin of θ_{VB} are averaged together in order to obtain the distribution of $\sigma_m(\theta_{VB}, \tau)$. In our case, the angular step of this distribution is 1° wide.

The results of this polarization analysis are shown in Figure 2. Each panel in the right-hand column shows the speed profile of the same high-speed stream and the locations of the analyzed 12hr time intervals (see Table 1 for a detailed list of intervals). The distributions of $\sigma_m(\theta_{VB}, \tau)$ are shown in the corresponding panels in the left-hand column.

The first time interval shows a clear right-handed signature around 90° and a less extended left-handed signature around 180°. The 99% confidence level is indicated by the solid black contour lines. The probability that the results encircled by these contours might be obtained by pure chance is only 1% (see Telloni et al. 2015 for a detailed discussion).

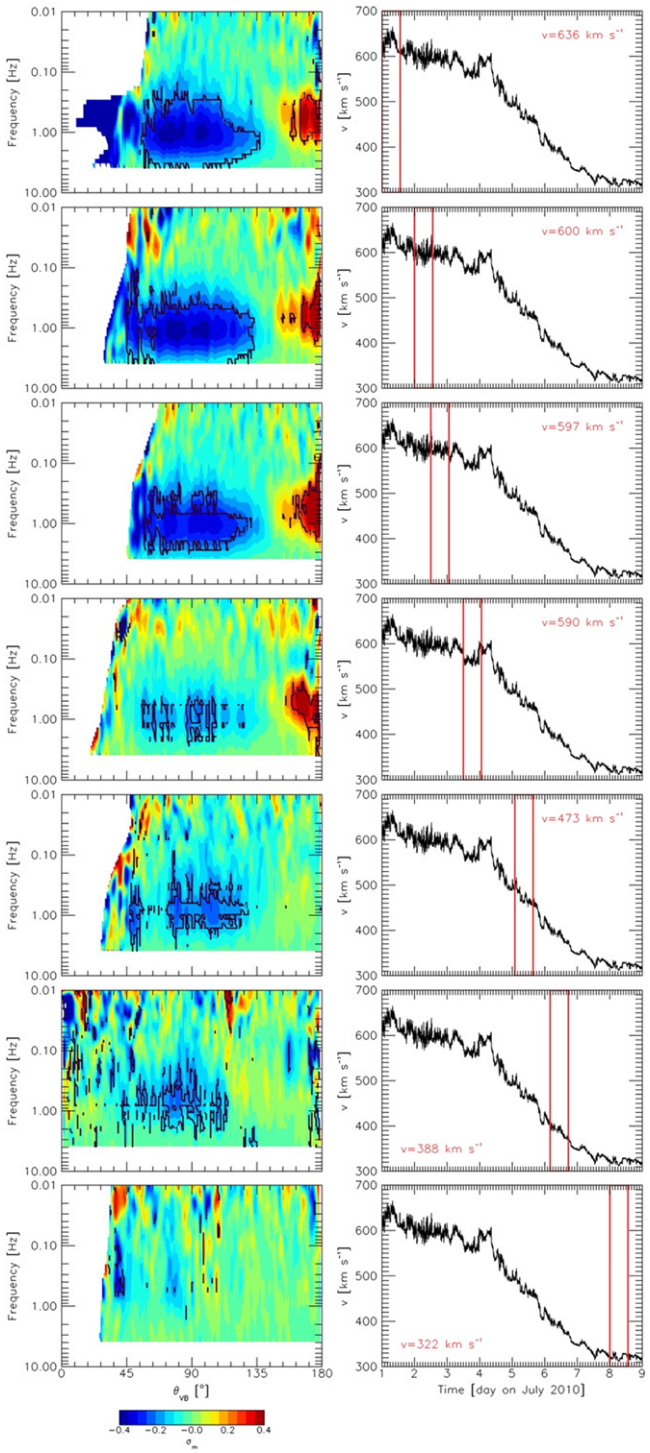

Figure 2. Distributions of the normalized magnetic helicity spectrum with respect to the angle θ_{VB} between the orientations of the local mean magnetic field and the sampling direction (left), observed in the transition from fast to slow wind (from top to bottom). The black contour lines show the 99% confidence levels. The regions of interest of the analysis along the wind speed profile (right) are enclosed by red boxes; the average speed of the solar wind in each time interval is also reported.

The color saturation indicates that these two populations are strongly polarized. As already reported in the literature (He et al. 2011, 2012a, 2012b; Podesta & Gary 2011; Telloni et al. 2015), the right- and left-handed polarized magnetic fluctuations, sampled quasi-perpendicularly and quasi-antiparallely to the local magnetic field direction, should be associated with KAWs and Alfvén-ion-cyclotron waves, respectively.

Table 1
Starting Time and Average Solar Wind Speed V_{sw} of the Data Intervals Used in the Present Analysis; Each Interval Lasts 12 hr

Day of 2010 July	DoY (day)	Time (hh:mm)	V_{sw} (km s^{-1})
01	182	00:00	636
02	183	00:00	600
02	183	12:00	597
03	184	12:00	590
05	186	02:00	473
06	187	04:00	388
08	189	00:00	322

This polarization persists throughout the trailing edge of the stream where the Alfvénic correlation shown in Figure 1 is higher, although some decrease in the extension and the normalized magnetic helicity intensity can be noticed as we move along the speed profile. In particular, between the fourth and fifth intervals, i.e., when we enter the rarefaction region of the stream, the left-handed polarization is lost and the right-handed polarization is significantly reduced. As we move toward lower and lower speeds, we also begin to lose the right-handed polarized population to the extent that, in the last interval (bottom panel), our technique does not reveal the presence of any kind of polarized fluctuations.

However, we agree with He et al. (2011) that a possible bias in reduced magnetic helicity results in favor of all those fluctuations propagating (quasi) along the radial direction, i.e., the sampling direction. This needs to be accounted for in future studies estimating the relative contribution to the reduced magnetic helicity of those fluctuations propagating in different directions, i.e., at a given angle with the sampling direction.

This same technique allows us to estimate the power associated with the highly oblique and quasi-antiparallel polarized fluctuations with respect to the local mean field direction. To do this, we averaged the total power spectrum of the magnetic fluctuations (not shown) in angular intervals around $\theta_{VB} \sim 90^\circ$ and close to $\theta_{VB}180^\circ$, respectively, i.e., within the intervals [70°–110°] and [140°–180°], in order to include most of the two populations. For the quasi-parallel interval, we could not center the 180° value in the middle because, in our case, there are no estimates available at small angles with respect to the magnetic field direction.

The left and right panels of Figure 3 show the power spectral density for the perpendicular and parallel fluctuations, respectively, within the various time intervals corresponding to the solar wind samples shown in the right-hand columns of Figure 2. The different time intervals are indicated by different colors.

The power density spectra for both perpendicular and parallel fluctuations, $P_\perp$ and $P_\parallel$, respectively, are generally higher within the fast trailing edge of the stream if compared to the slower rarefaction region. As a matter of fact, the first four intervals show the highest spectral density. Within the inertial range, the parallel and perpendicular fluctuations approximately share the typical $-5/3$ Kolmogorov scaling (Kolmogorov 1941), regardless of the analyzed wind sample, either fast or slow, but the perpendicular power is generally larger, as

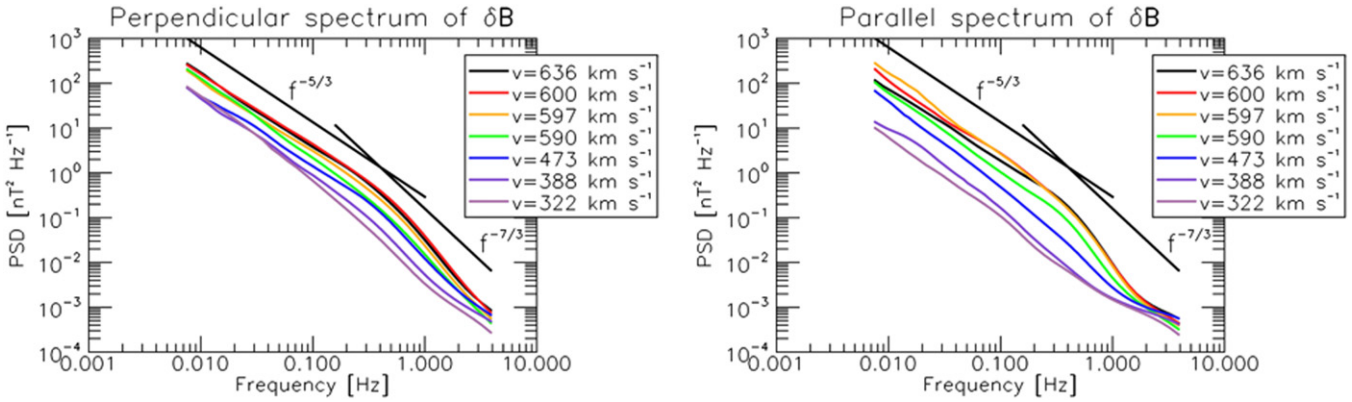

Figure 3. Power spectral density (PSD) of perpendicular (left-hand side panel) and parallel (right-hand side panel) magnetic fluctuations as inferred along the high-speed stream; different colors are used for different solar wind samples characterized by different average speeds as reported in both panels. Scalings of $-5/3$ (typical of the Kolmogorov turbulence, Kolmogorov 1941) and $-7/3$ (expected for the incompressible Hall effect, Galtier & Buchlin 2007) for the fluid and kinetic ranges, respectively, are shown for reference in both panels.

predicted by Goldreich & Sridhar (1995) for anisotropic turbulence, although a more direct comparison would require narrower angular bins as in Horbury et al. (2008).

At frequencies beyond the spectral break located at 0.3–0.4 Hz, $P_{\parallel}$ is generally steeper than $P_{\perp}$. In addition, as already reported in the literature (Bruno et al. 2014), a large variability of the spectral index is observed at proton scales. The value of the spectral index depends on the power associated with the fluctuations within the inertial range: the higher the power, the steeper the slope.

In Figure 4, we report the ratio between the perpendicular $P_{\perp}$ and parallel $P_{//}$ power density, having averaged together the first four spectra within the high-speed trailing edge. This ratio shows an anisotropy in favor of $P_{\perp}$ throughout the frequency range. In particular, this anisotropy increases for increasing frequency and, around 1 Hz, reaches its maximum value before decreasing dramatically immediately after. These results are qualitatively similar to those obtained by Podesta (2009). In our case, the maximum value of this ratio coincides with the frequency location of the core of the KAW population, which is at a slightly higher frequency with respect to the core of the parallel population.

Finally, Figure 5 reports the results for the intermittency analysis of the magnetic field intensity and vector fluctuations for the same time intervals listed in Table 1. For details on the methodology based on the flatness, and for a review on previous intermittency results related to magnetic field fluctuations within both the fast and slow wind, the reader can refer to the paper by Bruno et al. (2003).

For each time interval, we show values for the flatness of the distributions of the magnetic field intensity and vector differences versus timescale.

In the left-hand panel, the flatness increases for all of the intervals when we move from large to small scales, reaching its maximum at scales slightly larger than the inverse of the frequency break which, in this case, is around 0.3–0.4 Hz (Bruno & Trenchi 2014). Beyond this frequency, all of the curves experience a rapid decrease toward the Gaussian value of the flatness. There is not much order in the way the curves are organized in the plot. Following the definition of intermittency given by Frisch (1995), i.e., the same time series is defined to be more intermittent if the flatness grows faster with decreasing scale, it is rather difficult to establish reliably which curve is more intermittent.

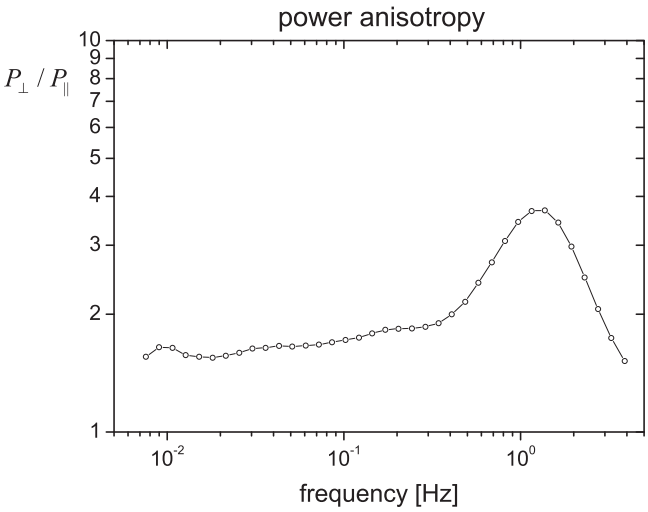

Figure 4. Anisotropy ratio between the perpendicular $P_{\perp}$ and parallel $P_{//}$ power density. See the text for details.

On the contrary, the same parameter computed for directional fluctuations, shown in the right-hand panel, shows that the flatness of the slow wind starts to increase before that of the fast wind, confirming the more intermittent nature of its magnetic fluctuations (Marsch & Liu 1993; Bruno et al. 2003). Moreover, again at odds with compressive fluctuations, the decrease of these curves seems to take place at slightly smaller scales, closer to the inverse of the frequency break.

3. DISCUSSION AND CONCLUSIONS

The character of the fluctuations within roughly the first decade of frequency beyond the high-frequency break separating the fluid and kinetic regimes strongly depends on the wind type. Our analysis indicates that both the wind speed and Alfvénicity are valid discriminants, as we found remarkable differences between the fast and slow wind. We find a clear signature of both KAW and ion-cyclotron waves within those regions of the trailing edge characterized, at fluid scales, by large fluctuations with a strong Alfvénic character. As a matter of fact, the first four intervals, characterized by similar Alfvénicity and similar amplitude of the fluctuations, show rather similar fluctuations at kinetic scales but, as soon as the

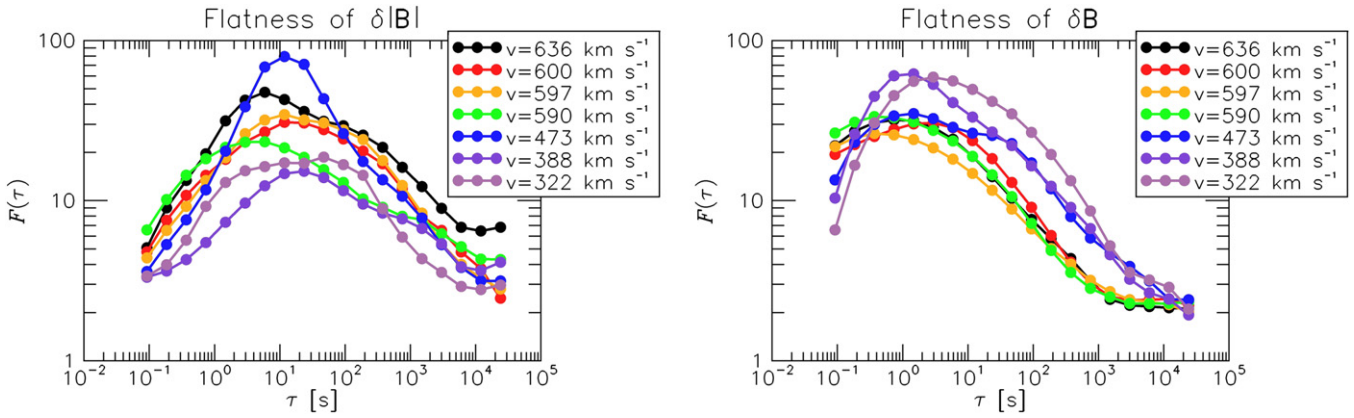

Figure 5. Left-hand panel: flatness factor vs. timescale τ, relative to fluctuations of the magnetic field intensity observed within the time intervals reported in Table 1; the legend reports the average speed and the corresponding color for each time interval. Right-hand panel: flatness factor relative to fluctuations of the magnetic field vector in the same format as of the left-hand panel.

corresponding Alfvénic correlation C_{VB} and the fluctuations' amplitude decrease, the polarization signature of these fluctuations is clearly depleted. Moreover, as we enter the rarefaction region and move toward slower regions, not only does the ion-cyclotron helicity signature disappear, followed by a more gradual disappearance of the KAW, but parallel and perpendicular spectral analyses also reveal that the associated power strongly decreases. In addition, the spectral analysis has not shown meaningful differences between the spectral indices related to parallel and perpendicular fluctuations within the inertial range since both classes of fluctuation seem to follow roughly a $-5/3$ scaling. Following the critical balance predictions (Goldreich & Sridhar 1995), we would expect a scaling of -2 for parallel fluctuations and $-5/3$ for the perpendicular ones, but our time intervals are probably too short and the angular bins too wide to allow for this kind of comparison. Nevertheless, there is no doubt that there is clear anisotropy in favor of the perpendicular spectrum and, at least within the kinetic regime, the parallel spectrum is the one that experiences the largest decrease, as also shown by the faster disappearance of the left-handed fluctuations. One possible mechanism for the disappearance of the fluctuations with $k_{\parallel}$ might be the ion-cyclotron resonance which was recently re-invoked as a possible dissipation mechanism by Bruno & Trenchi (2014 and references therein). On the other hand, the depletion of KAW seems to be less dramatic since their polarization signature tends to survive in a large fraction of the rarefaction region. The intermittency observed within the various time intervals is consistent with the results already reported in the literature (Wu et al. 2013; Telloni et al. 2015). For each of the analyzed time intervals, the flatness increases from large to small scales down to scales corresponding roughly to the high-frequency break (see discussion in the previous section). However, around and beyond the frequency break, the flatness starts to decrease. In particular, we note that while compressive fluctuations become less intermittent well before the frequency break, as already reported by Wu et al. (2013), directional fluctuations have a much slower decrease which starts around the frequency break. We believe that there might be some connection between this observation and the fact that the central part of the KAW and Alfvén-ion-cyclotron populations is generally located at scales slightly smaller than that corresponding to the spectral break as reported in Figure 2 from Telloni et al. (2015). However, this conclusion needs to be corroborated by further investigations since it seems not to be supported by the fact that while in slow wind the signatures of both KAW and ion-cyclotron waves gradually disappear, we still register a roughly similar behavior of intermittency. Within slow wind there is probably still some residual population of KAW and ion-cyclotron waves that our analysis is not able to unravel because of the low level of the corresponding signals.

This research was partially supported by the Italian Space Agency (ASI) under contracts I/013/12/0 and I/022/10/2, and by the European Commission's Seventh Framework Program under the grant agreement STORM (project No. 313038). Data from *WIND* were obtained from NASA-CDAWeb website.

REFERENCES

Alexandrova, O., Carbone, V., Veltri, P., & Sorriso-Valvo, L. 2008, ApJ, 674, 1153
Alexandrova, O., Chen, C. H. K., Sorriso-Valvo, L., Horbury, T. S., & Bale, S. D. 2013, SSRv, 178, 101
Bavassano, B., Pietropaolo, E., & Bruno, R. 1998, JGR, 103, 6521
Bruno, R., & Carbone, V. 2013, LRSP, 10, 2
Bruno, R., Carbone, V., Sorriso-Valvo, L., & Bavassano, B. 2003, JGR, 108, 1130
Bruno, R., Pietropaolo, E., Servidio, S., et al. 2008, AGU Fall Meeting (San Francisco, CA: AGU), Abstract SH42A-06
Bruno, R., & Trenchi, L. 2014, ApJL, 787, L24
Bruno, R., Trenchi, L., & Telloni, D. 2014, ApJL, 793, L15
D'Amicis, R., & Bruno, R. 2015, ApJ, 805, 84
Denskat, K. U., Beinroth, H. J., & Neubauer, F. M. 1983, JGR, 54, 60
Frisch, U. 1995, Turbulence: The Legacy of A. N. Kolmogorov (New York: Cambridge Univ. Press)
Galtier, S., & Buchlin, E. 2007, ApJ, 656, 560
Gary, S. P., & Borovsky, J. E. 2004, JGR, 109, 6105
Gary, S. P., & Smith, C. W. 2009, JGR, 114, A12105
Goldreich, P., & Sridhar, S. 1995, ApJ, 438, 763
Goldstein, M. L., Roberts, D. A., & Fitch, C. A. 1994, JGR, 99, 11519
Hamilton, K., Smith, C. W., Vasquez, B. J., & Leamon, R. J. 2008, JGR, 113, A01106
He, J., Marsch, E., Tu, C., Yao, S., & Tian, H. 2011, ApJ, 731, 85
He, J., Tu, C., Marsch, E., & Yao, S. 2012a, ApJ, 749, 86
He, J., Tu, C., Marsch, E., & Yao, S. 2012b, ApJL, 745, L8
Horbury, T. S., Forman, M., & Oughton, S. 2008, PhRvL, 101, 175005
Hundhausen, A. J. 1972, Coronal Expansion and Solar Wind (Physics and Chemistry in Space, Vol. 5; Berlin: Springer)
Karimabadi, H., Roytershteyn, V., Wan, M., et al. 2013, PhPl, 20, 012303
Kiyani, K. H., Chapman, S. C., Khotyaintsev, Y. V., Dunlop, M. W., & Sahraoui, F. 2009, PhRvL, 103, 075006
Kiyani, K. H., Chapman, S. C., Sahraoui, F., et al. 2013, ApJ, 763, 10

Kolmogorov, A. N. 1941, DoSSR, 30, 301
Leamon, R. J., Smith, C. W., Ness, N. F., Matthaeus, W. H., & Wong, H. K. 1998, JGR, 103, 4775
Lepping, R. P., Acũna, M. H., Burlaga, L. F., et al. 1995, SSRv, 71, 207
Marsch, E. 2006, LRSP, 3, 1
Marsch, E. 2012, SSRv, 172, 23
Marsch, E., & Liu, S. 1993, AnGp, 11, 227
Marsch, E., Schwenn, R., Rosenbauer, H., et al. 1982, JGR, 87, 52
Matteini, L., Horbury, T. S., Neugebauer, M., & Goldstein, B. E. 2014, GeoRL, 41, 259
Matthaeus, W. H., & Goldstein, M. L. 1982, JGR, 87, 6011
Ogilvie, K. W., Chornay, D. J., Fritzenreiter, R. J., et al. 1995, SSRv, 71, 55
Narita, Y., Kleindienst, G., & Glassmeier, K.-H. 2009, AnGeo, 27, 3967
Perri, S., Goldstein, M. L., Dorelli, J. C., & Sahraoui, F. 2012, PhRvL, 109, 191101
Podesta, J. J. 2009, ApJ, 698, 986
Podesta, J. J., & Gary, S. P. 2011, ApJ, 734, 15
Salem, C. S., Howes, G. G., Sundkvist, D., et al. 2012, ApJL, 745, L9
Servidio, S., Valentini, F., Califano, F., & Veltri, P. 2012, PhRvL, 108, 045001
Sahraoui, F., Goldstein, M. L., Robert, P., & Khotyaintsev, Y. V. 2009, PhRvL, 102, 231102
Telloni, D., Bruno, R., & Trenchi, L. 2015, ApJ, in press
TenBarge, J. M., Podesta, J. J., Klein, K. G., & Howes, G. G. 2012, ApJ, 753, 107
Torrence, C., & Compo, G. P. 1998, BAMS, 79, 61
Tu, C.-Y., & Marsch, E. 1995, SSRv, 73, 1
Turner, A. J., Gogoberidze, G., Chapman, S. C., Hnat, B., & Müller, W.-C. 2011, PhRvL, 107, 095002
Wan, M., Matthaeus, W. H., Karimabadi, H., et al. 2012, PhRvL, 109, 195001
Wu, P., Perri, S., Osman, K., et al. 2013, ApJL, 763, L30